Evaluation of common mixing models for calculating bulk thermal conductivity of sedimentary rocks: Correction charts and new conversion equations

Sven Fuchs*, Felina Schütz, Hans-Jürgen Förster, Andrea Förster

GFZ German Research Centre for Geosciences, Section 4.1: Reservoir Technologies, Telegrafenberg, 14473 Potsdam, Germany

ARTICLE INFO

ABSTRACT

Different numerical models can be deployed to calculate the matrix thermal conductivity of a rock from the bulk thermal conductivity (BTC), if the effective porosity of the rock is known. Vice versa, using these parameters, the BTC can be determined for saturation fluids of different thermal conductivity (TC). In this paper, the goodness-of-fit between measured and calculated BTC values of sedimentary rocks has been evaluated for two-component (rock matrix and pores) models that are used widely in geothermics: arithmetic mean, geometric mean, harmonic mean, Hashin and Shtrikman mean, and effective-medium theory mean. The examined set of samples consisted of 1147 TC data in the interval 1.0–6.5 W m^{-1} K^{-1}. The quality of fit was studied separately for the influence of lithotype (sandstone, mudstone, limestone, dolomite), saturation fluid (water and isooctane), and rock anisotropy (parallel and perpendicular to bedding). From the studied models, the geometric mean displays the best, however not satisfying correspondence between calculated and measured BTC. To improve the fit of all models, respective correction equations are calculated. The "corrected" geometric mean provides the most satisfying results and constitutes a universally applicable model for sedimentary rocks. In addition, the application of the herein presented correction equations allows a significant improvement of the accuracy of existing BTC data calculated on the basis of the other mean models. Finally, lithotype-specific conversion equations are provided permitting a calculation of the water-saturated BTC from data of dry-measured BTC and porosity (e.g., well log derived porosity) with no use of any mixing model. For all studied lithotypes, these correction and conversion equations usually reproduce the BTC with an uncertainty < 10%.

© 2013 Elsevier Ltd. All rights reserved.

1. Introduction

In geothermal studies, the rock thermal conductivity (TC) constitutes an important parameter. It is essential for the determination of the heat flow from the Earth's interior and is indispensable in any thermal modeling. In sedimentary-basin research, large databases of TC are required to characterize the major lithotypes making up the different geological formations and hence entire sedimentary sections. The amount of data needed to characterize fully a sedimentary setting thereby depends on the geological history and associated facies changes and may be large.

The most reliable TC values originate from direct laboratory measurements. If core samples are not available, indirect methods are used to calculate TC from petrophysical properties, including porosity, a parameter provided through well logging (e.g., Balling et al., 1981; Goss and Combs, 1976; Goutorbe et al., 2006; Hartmann et al., 2005). Another indirect approach of TC determination uses

the abundance and composition of the rock-forming minerals and the porosity as a multi-component system (e.g., Brailsford and Major, 1964; Brigaud et al., 1990; Demongodin et al., 1991; Vasseur et al., 1995). All these indirect methods have their shortcomings and restrictions.

Various laboratory methods for the measurement of TC are available comprising steady-state techniques (e.g., divided bar technique, needle probe) and transient techniques (e.g., line-source methods, ring-source methods, optical scanning). Comprehensive reviews on these techniques are provided by Kappelmeyer and Haenel (1974), Beck (1988), Blackwell and Steele (1989), and Somerton (1992). The less time-consuming optical scanning technique (OS) is, since introduced in the 1990s by Y. Popov, recently the most frequently used method to measure TC for large sample sets. This method was applied successfully to crystalline rocks (e.g., He et al., 2008; Popov et al., 1999) as well as to sedimentary rocks (e.g., Clauser, 2006; Fuchs and Förster, 2010; Hartmann et al., 2005, 2008; Homuth et al., 2008; Liu et al., 2011; Majorowicz et al., 2008; Mottaghy et al., 2005; Norden and Förster, 2006; Orilski et al., 2010; Popov et al., 1995, 2003, 2010, 2011; Schütz et al., 2012). It involved the measurement of TC under ambient temperature and pressure, which is in contrast to the other widely used method,

---

* Corresponding author. Tel.: +49 331 288 2842; fax: +49 331 288 1450.
  E-mail address: fuchs@gfz-potsdam.de (S. Fuchs).

the divided-bar technique (DB). This method obtains TC applying uniaxial pressure. Measurements under pressure have the advantage that micro cracks that may have originated from decompression and cooling as result of borehole drilling or rapid uplift, will get closed. The presence of micro cracks would cause underestimation of TC compared to an intact sample, whereby the rate of underestimation strongly depends on the type of saturation (air or water). Schärli and Rybach (1984) showed that because of micro cracks, the difference between dry and water-saturated TC in granitic rocks may be as high as 30%. For saturated metamorphic rocks (gneiss and amphibolite), the comparison of TC obtained by the DB and OS methods resulted in small discrepancies (AME < 3%), although an axial load of 4–6 MPa was applied in the DB approach (Popov et al., 1999). An analog study for sedimentary rocks is missing. However, despite this circumstance we are confident that the approach of this paper, which is entirely based on OS results, is scientifically sound.

To perform the laboratory work economically, i.e., studying large sample numbers in affordable time, measurements are usually performed in dry state, with air as the pore-saturating medium. Additional effort then is needed to convert these TCs to values typical for e.g., aquifers with water as the pore-filling fluid or hydrocarbon reservoirs, in which the rock contains either water, oil, or gas, or a mixture of those. The calculation of the rock TC for different saturation fluids then requires the use of mixing models.

In general, those multi-component mixture models to describe the TC of a rock can be grouped in (1) well-defined physical (often referred as structural or theoretical) models and in (2) purely empirical or semi-empirical approaches. A third group of models is based on numerical simulations. Physical models may have a wider applicability (depending on the degree of simplification to obtain a solution), but their usability is often limited by the inclusion of empirically determined parameters, compositional variations, or structural aspects (e.g., Popov et al., 2003; Schopper, 1991; Sugawara and Yoshizawa, 1961; Zimmerman, 1989). Empirical models have the drawback that they are strictly valid for the particular rock suite being used for model development. Extensive overviews of TC models are provided by Tinga et al. (1973) and Progelhof et al. (1976) (for two-component mixtures) as well as by Abdulagatova et al. (2009).

Rather simple models, easily and comfortably applied, are based on a two-phase system of the rock comprising the solid mineral matrix and the pore space. Thus, if porosity and bulk TC (BTC) of a sample are measured, a matrix TC (MTC) can be inferred for the sample and in turn a BTC for another pore fluid with different TC calculated.

This paper provides a validity study of simple and usually used mixing models for a two-phase rock system involving (1) the layered medium model (series and parallel model corresponding to the arithmetic and harmonic means and the mean of both), (2) an empirical model not relying on any physical theory (the geometric mean), (3) the Hashin and Shtrikman mean, the upper and lower bounds of which provide tighter constraints than the arithmetic and harmonic means, and (4) the effective medium mean (based on the effective-medium theory). The selection of these models builds on results of Clauser (2009), who discussed the performance of these mixing models for a fixed MTC and a variable porosity, however without validating the results with measured laboratory TC.

It was examined, which of the selected mixing models best describes the TC of sedimentary rocks. The evaluation considers three different aspects: (1) lithotype, (2) pore content (air, water, or other saturating fluids), and (3) anisotropy. The statistical analysis of the deviations between laboratory-measured and calculated BTC data comprises 1147 single values obtained from 717 samples of sandstone, mudstone, limestone, and dolomite. As a result of this statistical analysis, the paper provides correction equations that yield an improved fit for some of the examined models. Finally, we present conversion equations that permit calculation of the water-saturated BTC from the dry-measured BTC for the case that porosity is known, e.g., from petrophysical well logging. This approach has the advantage that a BTC could be inferred for a different saturating fluid without application of any mixing model.

2. Previous comparison studies

A verification of the different mathematical models, considering a solid and a pore volume, by comparison with real data has not yet been comprehensively performed. Most studies comparing between measured and calculated BTC values encompassed crystalline rocks.

Robertson and Peck (1974) compared BTC calculated from eleven theoretical mean models with TC values measured on 61 olivine-bearing basalt samples. None of the models showed a good agreement over the large range of porosity that the samples possessed (2–97%). The study showed on the one hand that a correction factor must be applied to the computed values to reduce the calculation error and on the other hand that the geometric-mean model belongs to those few approaches yielding the best, although unsatisfying, match. Horai (1991) reevaluated the data from Robertson and Peck (1974) and concluded that the mismatch in modeled and measured data is caused by errors introduced by the use of data from different measurement techniques.

More recently, Pribnow (1994) examined the four most widely used models (geometric mean, arithmetic mean, harmonic mean, and the Hashin and Shtrikman mean) for 85 water-saturated amphibolite and gneiss samples using the DB technique (Birch, 1950) and the line-source approach (Lewis et al., 1993). The geometric mean model, together with the mean of the arithmetic and harmonic mean models, provided the best fit.

Analog studies of the evaluated mean models focusing on sedimentary rocks are rare. Woodside and Messmer (1961b) used six sandstone samples to validate the geometric mean model for consolidated rocks and recognized a good agreement between predicted and measured BTC. Hutt and Berg (1968) analyzed several mean models (arithmetic mean, harmonic mean, geometric mean, Bruggeman, Maxwell, Rayleigh, Archie) for 28 sandstone samples. They compared the calculated BTC (using the TC of minerals for calculating the MTC) with values measured with a needle probe. The harmonic mean showed a good fit, whereas the arithmetic and geometric mean model overestimated the measured data. Buntebarth and Schopper (1998) explored various models for a suite of eleven sedimentary-rock samples saturated with different fluids (TC measurements with a needle probe). In their study, the application of the harmonic and arithmetic mean models resulted in a better fit relative to the geometric mean model. Clauser (2006) compared TC data of various sedimentary lithotypes with theoretical model curves and graphically identified the closest approximation of measured (using the OS technique) and calculated values for the geometric-mean model, except for limy sandstones. Several authors (e.g., Carson et al., 2005; Revil, 2000; Zimmerman, 1989) used the database of Woodside and Messmer (1961b) to test their own models for consolidated and unconsolidated rock. However, the number of data available for comparison was small and not comparable to the data set deployed in this study.

3. Methods applied

3.1. Models of two-phase systems

Calculation of the BTC (λ_b) of a two-component rock system involves the MTC (λ_m), the effective porosity (ϕ), and the TC of the pore content (λ_p).

3.1.1. Geometric mean

The empirical geometric-mean model (GM), which went back to Lichtenecker (1924) and was evaluated first by Woodside and Messmer (1961a,b) for consolidated sandstones and unconsolidated sands, represents the most usual approach. The empirical formula provides a relatively simple mathematical expression to calculate the BTC of a porous rock.

$$\text{GM}: \quad \lambda_b = \lambda_m^{1-\phi} \cdot \lambda_p^{\phi} \tag{1}$$

3.1.2. Arithmetic and harmonic mean

Other frequently applied approaches comprise the arithmetic-mean (AM) and harmonic-mean (HM) models, which both are based on a sheet model representing a layered structure of phases, where the heat flow passes either parallel (AM) or perpendicular (HM) with respect to the plane boundaries. The two models are independent of the pore structure and constitute special cases (boundaries) of Wiener's mixing law (Wiener, 1912), which applies to both isotropic and anisotropic mixtures. The models were introduced by Voigt (1928) and Reuss (1929) to define the upper and lower TC boundaries.

$$\text{AM}: \quad \lambda_b = (1-\phi) \cdot \lambda_m + \phi \cdot \lambda_p \tag{2}$$

$$\text{HM}: \quad \lambda_b = \frac{1}{((1-\phi)/\lambda_m) + (\phi/\lambda_p)} \tag{3}$$

3.1.3. Hashin and Shtrikman mean

The model of Hashin and Shtrikman (1962) (also referred as Maxwell–Eucken equations) is based on the theory of Maxwell (1892) and was extended by the work of Eucken (1940). It also uses upper (λ_{HS}^{U}; represents fluid-filled, spherical pores) and lower (λ_{HS}^{L}; represents grains suspended in a fluid) boundaries to calculate the TC of a two-phase system. The Hashin-and-Shtrikman bounds provide more restrictive narrower upper [Eq. (5)] and lower bounds [Eq. (7)] for isotropic mixtures, yet independent of the pore structure (Zimmerman, 1989). The mean of both bounds is often used as best approximation of rock BTC.

$$\lambda_b = \frac{1}{2}(\lambda_{HS}^{U} + \lambda_{HS}^{L}) \tag{4}$$

$$\lambda_{HS}^{U} = \lambda_m + \frac{\phi}{(1/(\lambda_p - \lambda_m)) + ((1-\phi)/3\lambda_m)} \tag{5}$$

$$\lambda_{HS}^{L} = \lambda_p + \frac{1-\phi}{(1/(\lambda_m - \lambda_p)) + (\phi/3\lambda_p)} \tag{6}$$

Solving Eq. (5) for λ_m produces a quadratic equation requiring the quadratic formula for the solution, which leads to two results but only one produces the real value [Eq. (8)].

$$\lambda_m = \frac{1}{2}(\lambda_{mHS}^{U} + \lambda_{mHS}^{L}) \tag{7}$$

$$\lambda_{mHS}^{U} = \frac{b + \sqrt{(b)^2 + 4 \cdot ac}}{2a} \tag{8}$$

$$a = 2(\phi - 1); \quad b = \lambda_{HS}^{U}(2 + \phi) - \lambda_p(1 + 2\phi); \quad c = \lambda_{HS}^{U}\lambda_p(1 - \phi)$$

$$\lambda_{mHS}^{L} = \frac{\lambda_p^2(2\phi) - \lambda_{HS}^{L} \cdot \lambda_p(3 - \phi)}{\lambda_{HS}^{L} \cdot \phi + \lambda_p \cdot (2\phi - 3)} \tag{9}$$

3.1.4. Effective-medium theory mean

To infer the TC for homogenous (isotropic) rocks, Bruggeman (1935) put forward the effective-medium theory (often referred as self-consistent medium approximation), which also uses the Lichtenecker (1924) formula. The effective-medium theory assumes different spherical inclusions embedded in a conducting host medium where all phases were mutually dispersed. This approach was further developed by Hanai (1968) and Sen et al. (1981) to the Bruggeman–Hanai–Sen equation for two-component systems. In this differential effective-medium theory the host phase percolates for the full range of fractions and the inclusions (second phase) may or may not conduct.

The effective-medium theory model is applicable to the determination of the TC of a multiphase system. Clauser (2009) transformed this equation to calculate the BTC for a two-component system [Eq. (10)] consisting of pore fluid and rock matrix:

$$\lambda_b = \frac{1}{4}\left\{ \begin{array}{c} 3\phi(\lambda_p - \lambda_m) + 2\lambda_m - \lambda_p \\ + \sqrt{\begin{array}{c} 9\phi^2\lambda_m^2 + 18\phi\lambda_m\lambda_p - 18\phi^2\lambda_m\lambda_p - 12\phi\lambda_m^2 \\ +\lambda_p^2 - 6\phi\lambda_p^2 + 4\lambda_m\lambda_p + 9\phi^2\lambda_p^2 + 4\lambda_m^2 \end{array}} \end{array} \right\} \tag{10}$$

Eq. (10) can be transposed to get MTC on its own [Eq. (11)]:

$$\lambda_m = \frac{\lambda_b(-2 \cdot \lambda_b + 3 \cdot \phi \cdot \lambda_p - \lambda_p)}{\lambda_b(3\phi - 2) - \lambda_p} \tag{11}$$

3.2. Anisotropy of thermal conductivity

The anisotropy of TC is a property that relates to the structure and texture of a rock, such as crystal anisotropy of the individual rock-forming minerals, intrinsic or structural anisotropy related to the shape of the grains and their textural arrangement, orientation and geometry of cracks, the spatial fracture distribution and other defects (Schön, 1996). For the quantification of anisotropy, TC is usually measured parallel ($\lambda_{||}$) and perpendicular ($\lambda_{\perp}$) to bedding or schistosity. The anisotropy ratio (A) then is defined as:

$$A = \frac{\lambda_{||}}{\lambda_{\perp}} \tag{12}$$

3.3. Methods of error calculation

To evaluate the reliability of the different mean models applied, the measured BTC is compared with the respective calculated BTC. For an individual sample, the deviation (E, in%) between calculated (λ_{cal}) and measured (λ_{mea}) TC is expressed as:

$$E = 100 \times \frac{|\lambda_{cal} - \lambda_{mea}|}{\lambda_{mea}} \tag{13}$$

For evaluating the different mean-model approaches, the arithmetic mean error (AME) was used to compare the calculated and the measured BTC:

$$\text{AME} = \frac{1}{n}\sum_{i=1}^{n} E_i \tag{14}$$

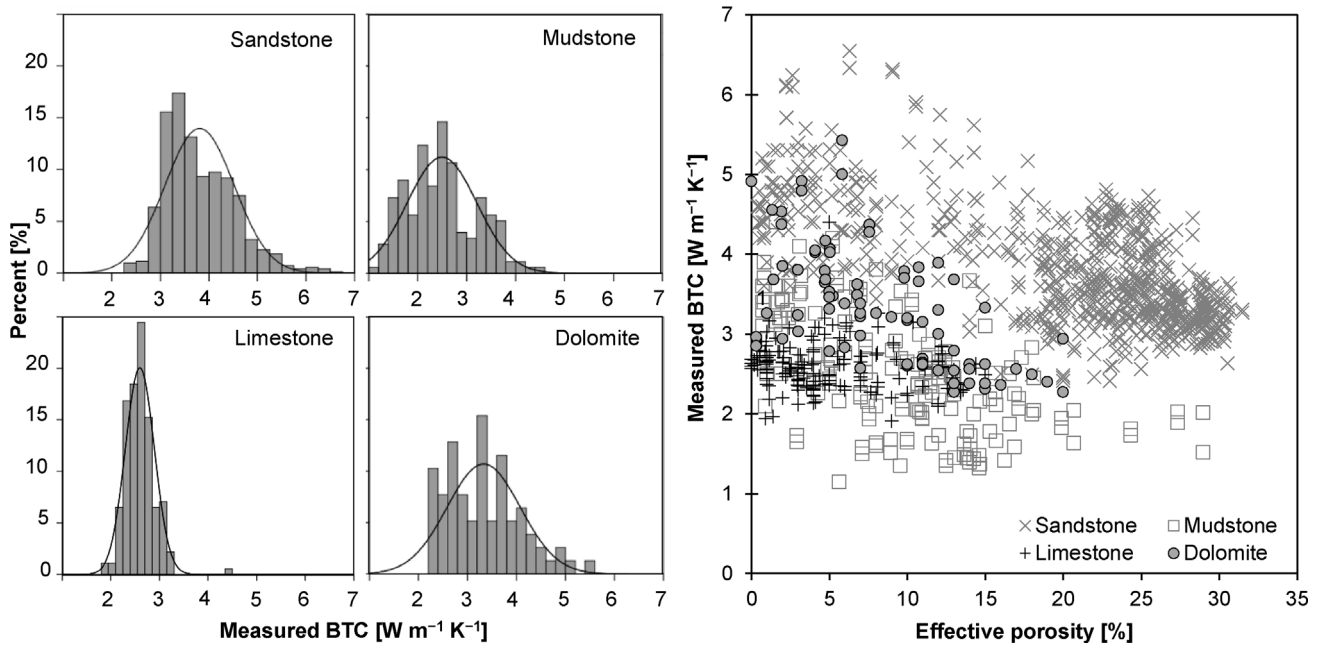where n is the number of samples in each lithotype group.

Fig. 1. Effective porosity and measured BTC (both water and isooctane-saturated) of the clastic and carbonate samples from this study.

In the following, the error is noted as the AME complemented by the respective 1σ standard deviation (SD). The AME can be expressed also as root mean square error (RMSE), which is a good measure of model accuracy, having the form:

$$\text{RMSE} = \sqrt{\frac{\sum_{i=1}^{n} E_i^2}{n}} \qquad (15)$$

The fit between predicted and measured data is statistically evaluated by regression analysis and the analysis of variances. The critical significance level α (mostly the statistical benchmark of 0.05), the observed significance level p, and the F-value constitute the key parameters for comparison (see Section 5.1).

4. The database

In total, 1147 TC measurements performed on 717 samples were evaluated. The database comprises four data sets from different sedimentary basins: (a) Mesozoic platform sediments of the northern Sinai Microplate in Israel (81 drillcore samples; Schütz et al., 2012), (b) the eastern part of the North German Basin [339 drillcore samples of the Mesozoic; Fuchs and Förster, 2010, 2013 (unpublished results); 129 drillcore samples of the Permo-Carboniferous; Norden and Förster, 2006]; and (c) the South German Scarplands and the Molasse Basin (168 drillcore and outcrop samples; Clauser et al., 2007). The studied samples encompass the following lithotypes: 137 limestone samples, 63 dolomite samples, 409 sandstone samples, and 108 mudstone (claystone + siltstone) samples. The TC data from these lithological subsets were scrutinized with respect to statistical distribution, and outliers (>2σ SD) were omitted in additional analyses.

All these TC data have in common that they were obtained with the Thermal Conductivity Scanning (TCS) apparatus (Lippmann and Rauen, GbR Schaufling, Germany), which is based on the high-resolution OS method (Popov et al., 1999). The sample size correlated with the drillcore diameter, which varied between 5 and 10 cm. Sample thickness was variable, but

exceeded the required minimal length of scanning lines of 4 cm. Measurements were performed on a flat sample surface displaying a roughness of <1 mm. The error of determination was less than 3%.

All samples were measured under ambient pressure and temperature, both dry (oven-dried at 60 °C) and water-saturated using distilled water. Determination of the anisotropy ratio of macroscopically isotropic samples involved TC measurement on the top/bottom of the cylindrical core and along the vertical core axis. For optically anisotropic samples, this ratio was calculated by measuring TC parallel and perpendicular to bedding (see Section 3.2). The effective porosity was quantified by the mass change between dry and water-saturated samples (Archimedes method). Because of clay-swelling effects, mudstones and argillaceous sandstones were saturated with isooctane (density: 0.698×10^3 kg m^{-3}; Budavari, 1989) instead of water to determine their porosity. TC values of 0.025 W m^{-1} K^{-1} for air (Gröber et al., 1955), 0.095 W m^{-1} K^{-1} for isooctane (Watanabe, 2003), and 0.604 W m^{-1} K^{-1} (Lemmon et al., 2005) for distilled water were used in the calculations.

Fig. 1 provides a compilation of measured BTC and effective porosity for the four lithotypes. The rocks covered a large range in effective porosity, from almost zero to about 30%. The carbonate rocks are usually less porous relative to the clastic rocks. Eighty percent of the entire data population of carbonates fall in the porosity range 1–13%, in contrast to 3–28% encompassed by the clastic rocks. As to the measured BTC, the sample suite spans the interval between 1.0 and 6.5 W m^{-1} K^{-1}. The larger variability in TC observed for sandstone (3.8 ± 0.7 W m^{-1} K^{-1}), mudstone (2.5 ± 0.7 W m^{-1} K^{-1}), and dolomite (3.3 ± 0.7 W m^{-1} K^{-1}) relative to limestone (2.6 ± 0.3 W m^{-1} K^{-1}) is a reflection of their greater heterogeneity in terms of modal mineralogy.

5. Results

The MTC was calculated from measured dry and saturated values for arithmetic, harmonic, and geometric means using Eq. (1)–(3) transposed to λ_m. Eqs. (7) and (11) were applied for the
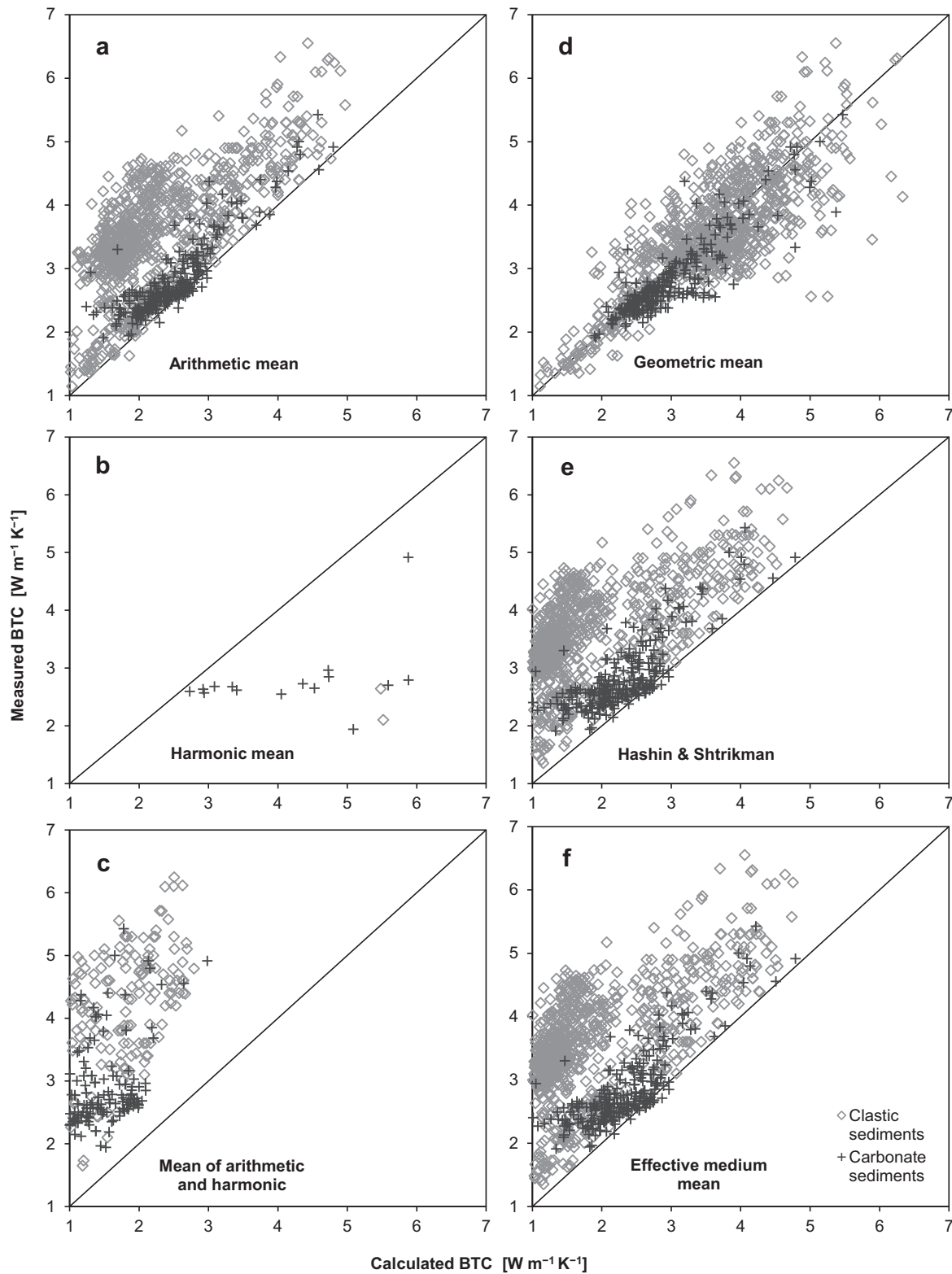
Fig. 2. Scatter plots of measured vs. calculated water-saturated BTC for clastic ($n = 885$) and carbonate sediments ($n = 262$).

Hashin–Shtrikman and the effective medium means, respectively. Water-saturated BTC for the various mixing models were subsequently calculated from Eqs. (1)–(4) and (10). The BTC results are shown as scatter plots for the six models (Fig. 2). Fig. 3 illustrates the influence of different saturation fluids (water and isooctane) on BTC.

5.1. General model fit

A regression analysis was performed to ascertain the model with the highest coefficient of determination (R^2). The results show that most of the evaluated mixing models predict the measured BTC unsatisfactorily. The highest value of R^2 is related to the
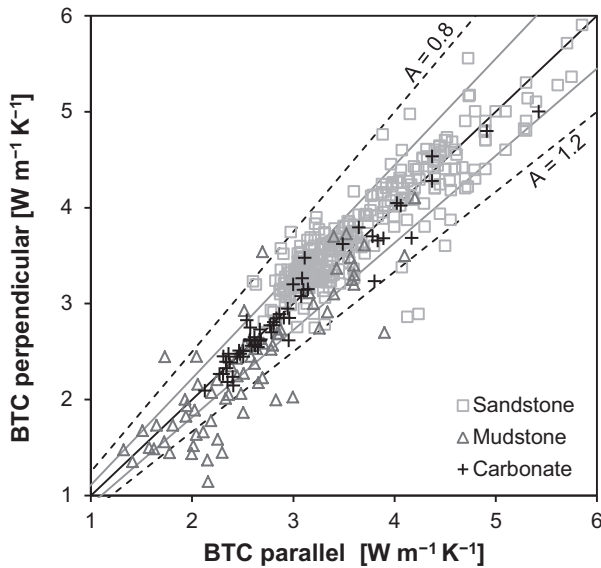
**Fig. 3.** Scatter plot of measured water-saturated BTC parallel and perpendicular. See text for explanation.

geometric mean ($R^2 = 0.62$, $F \sim 1348$). Significantly poorer fits are observed for the arithmetic mean ($R^2 = 0.37$, $F \sim 600$), followed by the effective medium mean ($R^2 < 0.24$, $F \sim 321$) and Hashin and Shtrikman mean ($R^2 = 0.23$, $F \sim 298$). The harmonic mean ($R^2 < 0.01$, $F = 1.56$) as well as the mean of arithmetic and harmonic mean ($R^2 = 0.01$, $F = 9.01$) show even lower coefficients of determination. If the value obtained for F is equal to or larger than the critical F-value, then the null hypothesis (H_0: $\mu_1 = \mu_2$) is rejected, and the result is significant at the chosen level of probability ($\alpha = 0.05$). This critical value is assumed to be $F_{crit}(1/1017) = 3.85$.

Fig. 2 shows the comparison between measured and calculated BTC for the different models. The arithmetic mean (Fig. 2a) tends to underestimate BTC in particular for clastic sediments (AME $33 \pm 20\%$), but yields an acceptable fit for carbonate samples (deviation $11 \pm 20\%$). The harmonic mean (Fig. 2b) consistently underestimates BTC and, with respect to the insignificant regression relation, is excluded from further discussion. This poor match also holds for the mean of arithmetic and harmonic means (Fig. 2c). The geometric mean (Fig. 2d) shows a reasonably good fit for both carbonate (AME $6 \pm 10\%$) and clastic (AME $5 \pm 17\%$) rocks. It tends to slightly overestimate BTC, but 80% of the samples show deviations $\leq 20\%$. The Hashin and Shtrikman mean (Fig. 2e) shows an acceptable fit for carbonate (AME $19 \pm 13\%$), but a poor fit for clastic rocks (AME $51 \pm 18\%$). Its overall distribution pattern largely corresponds to those of the arithmetic and effective medium means (Fig. 2f). Because these three models provided virtually the same goodness of fit (ANOVA, Tukey's HSD, $\alpha = 0.05$, $n = 1019$), the effective medium mean could be eliminated from further analysis.

5.2. Anisotropy of thermal conductivity

The vast majority of rock samples possess anisotropy ratios between 0.8 and 1.2 (Fig. 3). Whereas the carbonate rocks and most sandstone samples are largely isotropic (mean anisotropy ratio = 1.01 ± 0.05 and 0.97 ± 0.08, respectively), many mudstone samples are anisotropic, exposing a mean anisotropy ratio of 1.11 ± 0.19.

Rock samples showing an anisotropy >5% ($n = 424$) are evaluated in terms of a possible impact that anisotropy has on the mixing model that should be selected for calculation. A paired t-test was made to compare the average deviations of the predicted BTC with the BTC measured parallel and perpendicular to bedding.
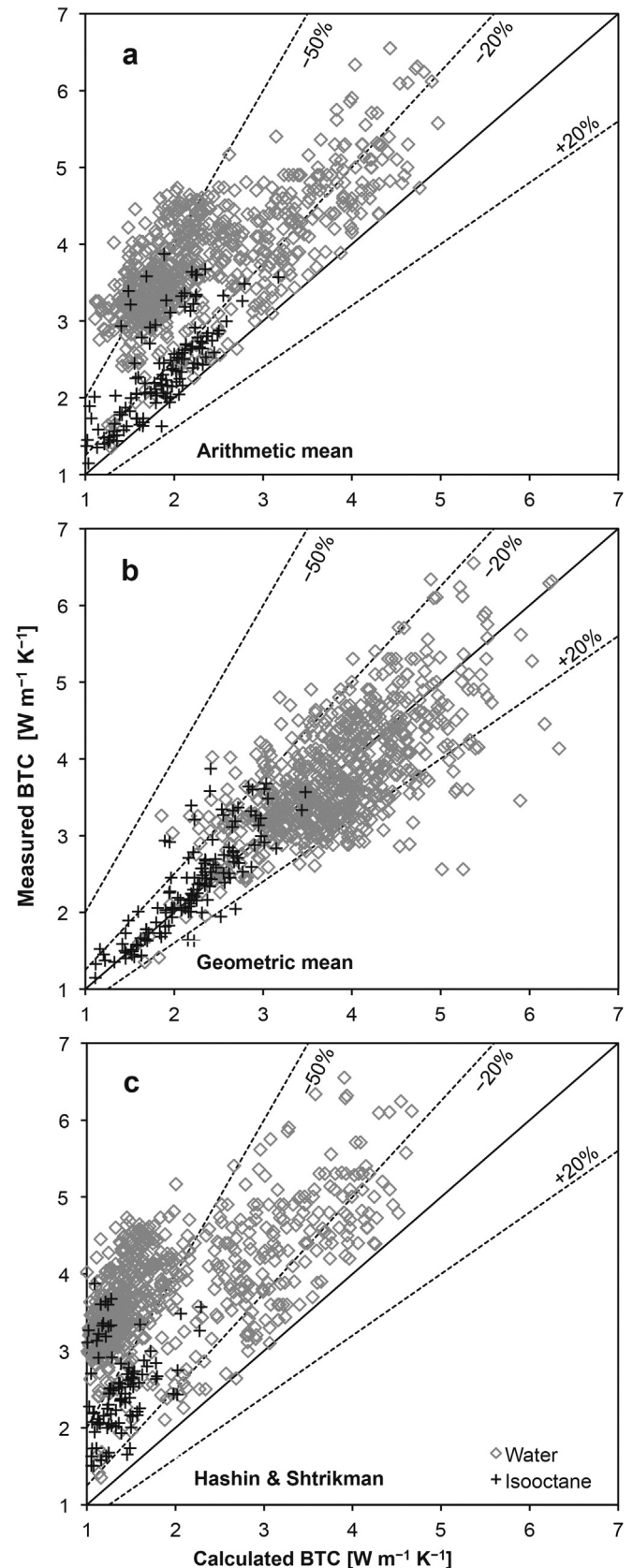
Fig. 4. Plots of measured BTC versus calculated BTC for water-saturated ($n = 757$) and isooctane-saturated ($n = 128$).
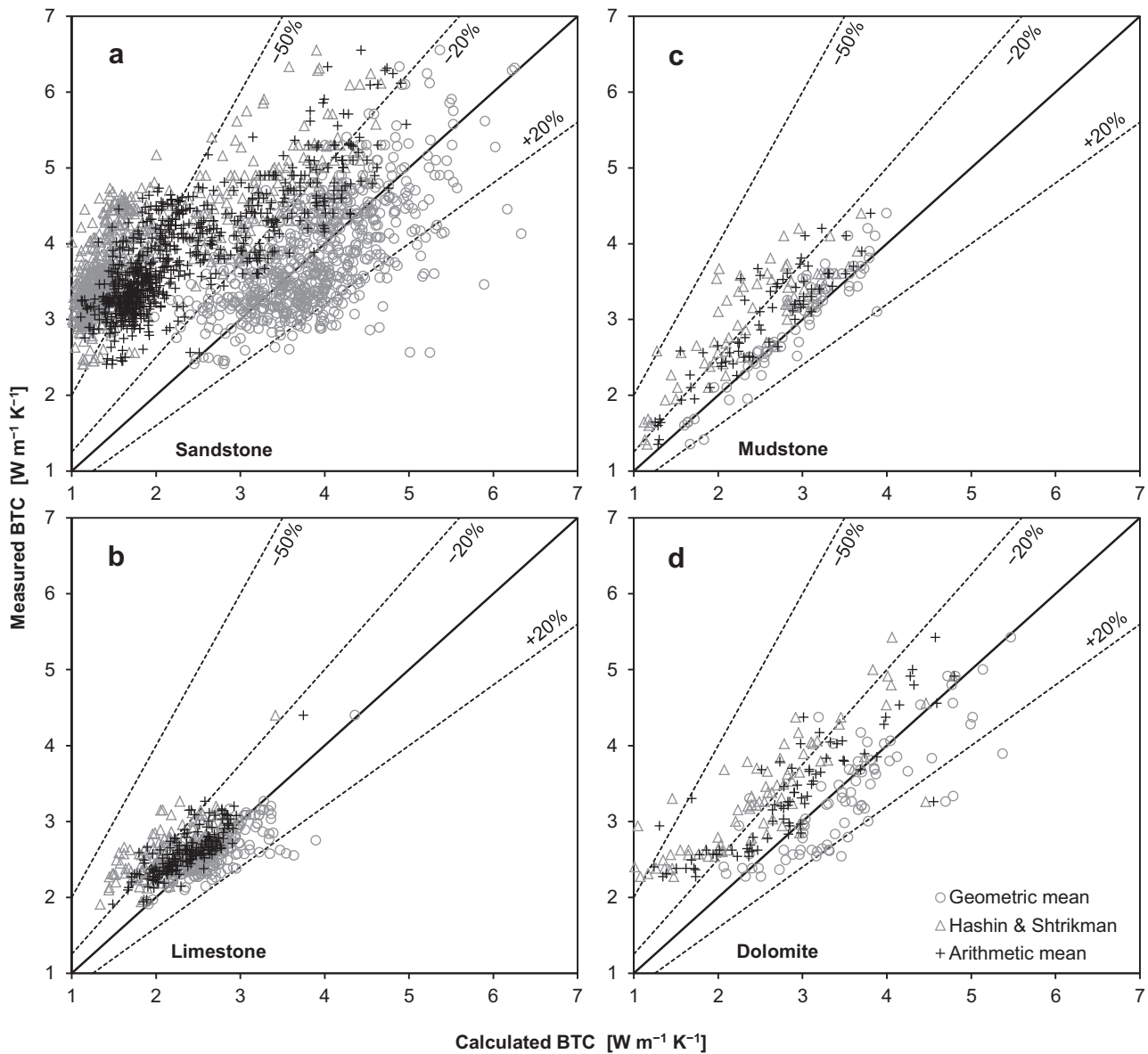
Fig. 5. Calculated BTC (water-saturated) based on different mixing models compared to measured BTC for different lithotypes.

Because the arithmetic-mean model is based on a sheet model with the heat flowing parallel to the components, it seemed reasonable to assume that this model will better fit the BTC parallel than perpendicular to bedding (harmonic mean) as well as those models that refer to isotropic media (the geometric and the Hashin and Shtrikman means).

However, the expectations are not met. For data referring to measurements parallel to bedding, the arithmetic mean model provides the same poor fit as for data related to measurements performed in the opposite direction (paired t-test, $n = 128$, $\alpha = 0.01$, $p = 0.425$). As to the geometric and Hashin and Shtrikman means, the results are in line with the theoretical background that the goodness of fit is basically the same for isotropic or anisotropic rocks.

5.3. Saturating fluid

The correlation between measured and calculated BTC of samples saturated with water or isooctane is displayed in Fig. 4. For

the range where measured TC values are available, the goodness of fit for samples saturated with isooctane is basically the same as for samples saturated with water. Accordingly, both the arithmetic and Hashin and Shtrikman means seriously underestimate BTC also for samples saturated with isooctane. For this saturation fluid, the geometric mean again shows the best fit (AME $6 \pm 6\%$).

5.4. Impact of lithotype

Fig. 5 shows the model-based relations between measured and calculated BTC for the different lithotype groups. For sandstones (Fig. 5a), only the geometric mean shows an acceptable fit (AME $13 \pm 11\%$), whereas the arithmetic and the Hashin and Shtrikman means strongly underestimate the BTC (AME $41 \pm 14\%$ and $53 \pm 16\%$, respectively). For limestones (Fig. 5b), the fit for the geometric and the arithmetic means is reasonably good (AME $6 \pm 5\%$ and $8 \pm 6\%$) and acceptable for the Hashin and Shtrikman mean (AME $12 \pm 9\%$). For mudstones (Fig. 5c), the geometric mean is the only approach resulting in a good fit. Both the arithmetic (AME

14 ± 9%) and the Hashin and Shtrikman means (AME 20 ± 12%) again underestimate the BTC, but less significantly. For dolomite, none of the models gave rise to a fit evaluated as good. An acceptable fit was obtained upon utilization of the geometric and arithmetic means (AME 12 ± 11% and 16 ± 12%, respectively).

6. Discussion

6.1. General model fit, anisotropy, and saturating fluid

The various mixing models evaluated in this study approximate measured BTC data in different, however mostly unsatisfying quality. Only the geometric mean consistently shows a good fit, with the bulk of calculated data deviating less than ±20% from measured BTC (Fig. 5). Considering the entire sample suite, the deviation averages between 11% (geometric mean) and 31% (arithmetic mean) and 42% (Hashin and Shtrikman mean). Only examining the lithotype, the deviation varies between 5.7% and 13% (geometric mean), 7.6% and 40% (arithmetic mean), and 12% and 53% (Hashin and Shtrikman mean). These results are in line with observations reported by Pribnow (1994) and Buntebarth and Schopper (1998). The latter authors rated the geometric mean model as best solution for situations, in which no additional criterion (e.g., an empirical alpha-value describing the pore structure of the rock) is considered.

Calculation of BTC with the harmonic mean [Eq. (3)] results in abnormal values (Fig. 2). More than 96% of the calculated BTC values are negative. This misfit, which was already recognized, for instance, by Beck and Beck (1965), Robertson and Peck (1974), and Pribnow (1994), can be attributed to the equation for calculating the MTC which allows the denominator to get zero or negative. Especially high porosities almost inevitably cause a negative denominator. Hence, this model is unfeasible and, with it, also the mean of the harmonic and arithmetic mean.

The goodness-of-fit and the effective porosity are antipathetically related also for the other models. This observation is linked with the mathematical formalisms of BTC calculation, causing greater uncertainties with increasing porosity.

For rocks with anisotropies >5%, the arithmetic-mean model did not show the expected correlation with the direction of measurement (i.e., the fit between measured and calculated TC should be better for data acquired parallel to bedding). The observations made in this study are just in opposition to this expectation and may question the physical concept of this model. This criticism is in line with earlier observations (e.g., Zimmerman, 1989) and implies that a body (rock) consisting of alternating slabs of matrix and pore space is physically unrealistic, at least for clastic sediments. The arithmetic-mean model, however, may apply for fractured aquifers in carbonate rocks in the situation of a layered fracture pattern. Moreover, because the bulk of our samples is only weakly anisotropic, the results of this study strictly apply only to rocks with anisotropies ≤20%. More strongly anisotropic rocks may fit the arithmetic-mean model better.

The use of isooctane (Fig. 4) has no statistically discernible impact on the quality of fit for either model (independent t-test, $\alpha = 0.05$, $p > 0.1$). The lower TC of isooctane compared to water and, hence, the smaller ratio between the TC of saturating fluid and air (factor ~3 for isooctane compared to factor ~24 for water) does not result in larger deviations between measured and predicted BTC, as one might expect. This observation is in contradiction to results of Buntebarth and Schopper (1998), who showed that the type of saturating fluid had a strong influence on the fitting of the geometric mean. These authors identified an acceptable fit for the geometric mean only for sandstone samples that were water-saturated ($n = 11$). More work is needed to explain this discrepancy.

Table 1
Coefficients of determination for correction charts shown in Fig. 6 (right panel).

	Mean model[a]	Regression parameter[b]			
		Type	b_0	b_1	R^2
Sandstone					
A	GM	linear	0.504	−3.039	0.927
B	AM	ln	2.091	0.340	0.887
C	H&S	ln	2.779	0.461	0.922
Mudstone					
D	GM	linear	0.208	−3.261	0.757
E	AM	ln	1.003	0.179	0.871
F	H&S	ln	1.502	0.282	0.941
Limestone					
G	GM	linear	0.059	−3.833	0.967
H	AM	ln	0.820	0.178	0.986
I	H&S	ln	1.378	0.301	0.976
Dolomite					
J	GM	linear	−0.104	−1.648	0.436
K	AM	ln	1.329	0.293	0.781
L	H&S	ln	1.869	0.388	0.909

[a] GM: geometric mean; AM: arithmetic mean; H&S: Hashin and Shtrikman.
[b] b_0 and b_1 are constants for regression model. Linear (linear) equation is $y = b_1 x + b_0$, logarithm equation (ln) is $y = b_1 \ln(x) + b_0$, where y is the calculated correction value and x is the given porosity value.

The re-calculation of isooctane-saturated BTC to water-saturated BTC is afflicted with several uncertainties. Therefore, saturation with water should be preferred to isooctane saturation in determining BTC. The use of isooctane or other alkanes, such as n-heptane utilized by Woodside and Messmer (1961b) and Zimmerman (1989), is an expedient alternative only for determining the porosity of argillaceous rocks.

In the special situation of handling BTC measured with different saturation fluids (air, water, n-heptane), we recommend averaging the respective matrix values. This recommendation is rooted in the observation of a significant difference in MTC calculated from dry-measured BTC (lower by 5.2%) compared to the matrix value calculated from isooctane-saturated BTC (paired t-test, $n = 127$, $\alpha = 0.05$, $p < 0.000$). A difference also is observed, but with an opposite trend, between MTC calculated from dry-measured BTC (higher by 4.9%) compared to the matrix value calculated from water-saturated BTC (paired t-test, $n = 1019$, $\alpha = 0.05$, $p < 0.000$).

6.2. Correction charts

The only mixing model that generally reproduces the measured BTC satisfactorily is the geometric mean, but the data scatter is still large. The other mean models examined in this paper produce TC data often significantly deviating from measured values. The question arises whether it is possible to calculate correction charts that permit reduction of the deviation and the scatter of the different mean models. In order to verify this idea, the relations between absolute deviation (in W m^{-1} K^{-1}) and porosity for the different lithotypes and mean models (Fig. 6a–d) are investigated. For this purpose, the data set is subdivided into porosity (%) classes: 0–3; 3–6; 6–10; 10–15; 15–20; 20–25; 25–30; 30–35 (Fig. 6e–h). The mean deviation within each porosity class is the input parameter for the regression analyses. The statistical treatment resulted in linear or logarithmic trend lines and respective equations, which in turn provided the correction values for every mean model and lithotype. For statistical reason, the initial data set was randomized into two groups. The first group (85% of data) is the regression set, from which the equations were derived; the second group (15% of data) is the testing set, from which the
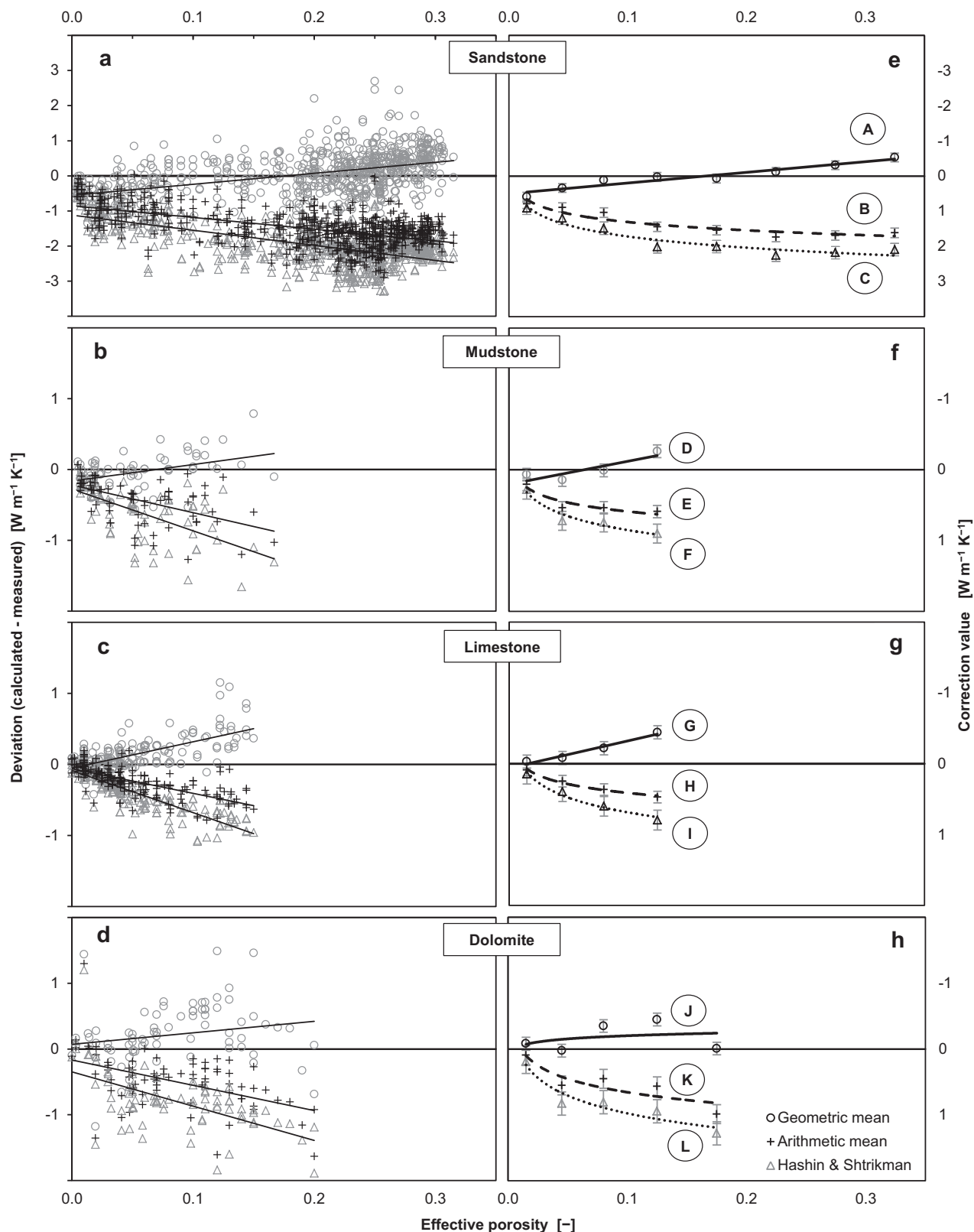
Fig. 6. Variations between calculated and measured BTC values (a–d) and derived correction values (e–h) for different lithotypes and mixing models, respectively. Regression coefficients and RMS values for A–L are listed in Table 1.

fitting parameters were calculated. The inversion of the curves shown in Fig. 6e–h gives the correction value (in W m^{-1} K^{-1}) for sandstone, mudstone, limestone, and dolomite, calculated by the arithmetic or geometric means. Table 1 is a compilation of the computed regression parameters for the various lithotypes and mean models. The correlation coefficients for the different groups scatter between 0.76 and 0.99, indicating a remarkably good degree of tracking. The only lithotype, for which the linear regression
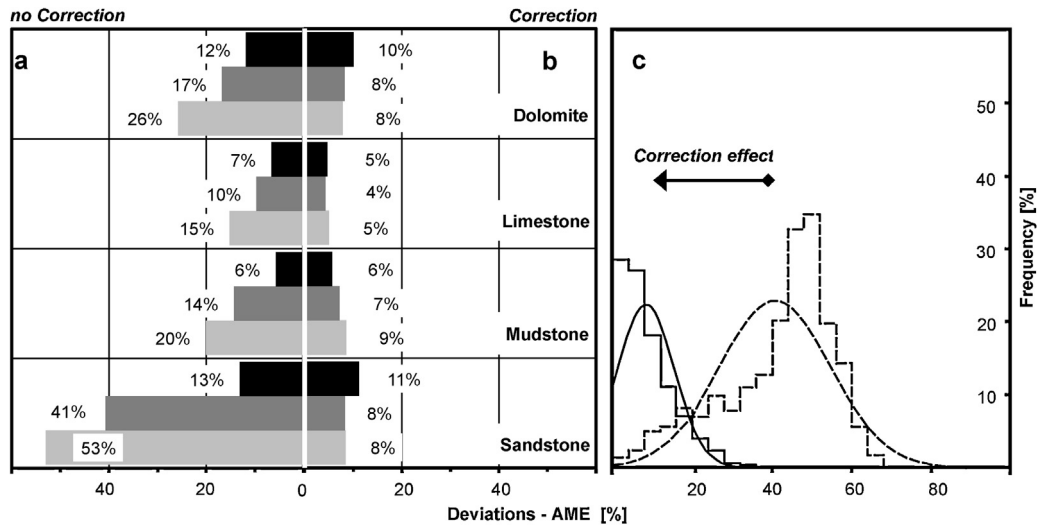
Fig. 7. Left: Comparison of corrected (b) (Fig. 6 and Table 1) and uncorrected (a) calculations. Black bar: geometric mean; dark gray bar: arithmetic mean; light gray bar: Hashin and Shtrikman mean. Right: Distribution of percent errors (c) for corrected (solid line) and uncorrected (dashed line) values for sandstones calculated with the arithmetic mean.

did not result in a satisfying improvement of the fit, is dolomite, with a quiet poor correlation coefficient of 0.43 for the geometric mean. The possible reason for this unsatisfying result is the fact that in our suite of dolomite rocks, the number of samples and the TC deviations in each porosity class are highly variable and, consequently, the calculated averages of deviation display larger uncertainties.

The impact of implementing these correction coefficients in the calculation of BTC is shown in Fig. 7a and b, separately for every model and lithotype. The application of the correction results in noticeable improvements of the fits for all mean models, on average reducing the deviations for the Hashin and Shtrikman equation by 70%, for the arithmetic mean by 59%, and for the geometric mean by another 15%. This improvement is exemplarily shown for the arithmetic mean used for BTC calculation of sandstone samples (Fig. 7c), exposing a smaller mean deviation and variance. In order to improve the applicability of the correction chart, mean deviations were converted to user-friendly correction values (Fig. 8). Those porosity-dependent correction values either have to be added to or subtracted from (depending on the algebraic sign) the original mixing-model results.

6.3. Conversion equations

The unsatisfying fitting behavior of most mean models and the necessity of applying correction charts encouraged us to examine our data set in whether is it possible to set up an equation that permits estimation of the water-saturated BTC directly from dry-measured BTC data and known porosity values.

For this goal, the data set was tested using a multiple regression analysis. The fitting result of this type of analysis is shown in Fig. 9. For statistical reasons, the initial data set was randomized into two groups of 85% (regression set) and 15% (testing set). The plot of measured versus predicted BTC shows a good fit for both the regression and the testing sets, with a deviation of $10 \pm 8\%$ (AME) for the testing set.

The coefficients of determination resulting from the multiple regression analysis are listed in Table 2 for the entire sample set and, additionally, for the various lithotypes. All listed equations display an AME equal or less than 10%. If the lithotype is sufficiently well known, we recommend application of the equations elaborated for mudstone, limestone, and dolomite instead of the one based on the entire set of samples, because the specific equations exhibit significantly lower AMEs (ANOVA, Tukey's HSD, $\alpha = 0.05$).
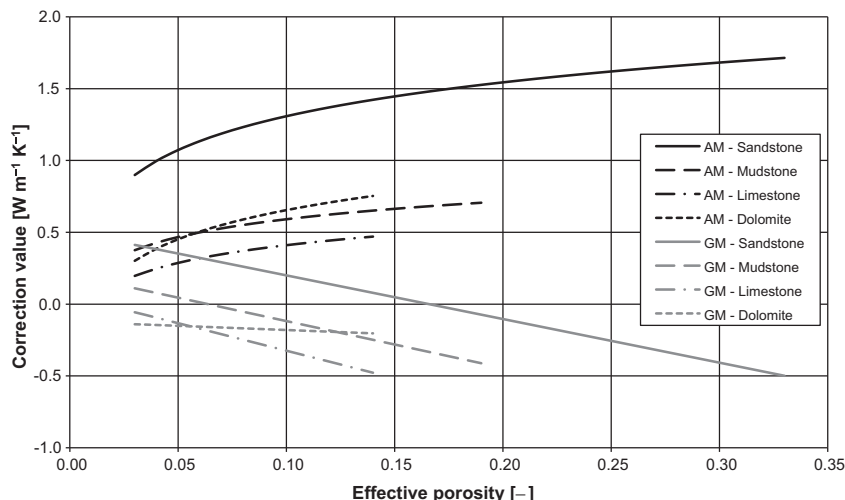

Fig. 8. Correction values for BTC calculation from dry measurements for sedimentary rocks. Arithmetic mean (AM): black lines, geometric mean (GM): gray lines.

Table 2
Results of multiple regression analyses of dry and saturated-measured BTC and effective porosity, respectively.

Samples	Regression parameter			R^2	ANOVA			AME
	b_o	b_1	b_2		F	n	p	
All	−0.406	7.417	1.216	0.726	1348.0	740/130	<0.001	10.2 ± 7.8%
Sandstone	1.579	2.244	0.817	0.667	581.4	494/87	<0.001	8.7 ± 7.2%
Mudstone	−0.696	8.446	1.290	0.895	243.9	51/8	<0.001	8.3 ± 7.7%
Limestone	0.272	3.961	0.914	0.758	243.2	134/23	<0.001	4.8 ± 4.3%
Dolomite	0.631	2.527	0.890	0.779	119.6	60/10	<0.001	6.5 ± 9.0%

b_0, b_1 and b_2 are constants for the multiple regression model. Equation is $y = b_1x + b_2z + b_0$, where y is the calculated BTC, x is the given porosity value and z is the dry TC. R^2 = coefficient of determination, F = F-value, n = number of samples (first value: regression set, second value: testing set), p = observed significance level, AME = arithmetic mean error ± 1 standard deviation for testing group.

Table 3
BTC mean errors as from correction equations and direct conversion equations.

Samples	Correction equations			Conversion equations
	AM	GM	H&S	
All	7.4 ± 6.9%	9.5 ± 9.5%	7.6 ± 7.0%	10.2 ± 7.8%
Sandstone	8.3 ± 7.2%	11 ± 10.2%	8.4 ± 7.2%	8.7 ± 7.2%
Mudstone	7.1 ± 7.3%	5.7 ± 4.9%	8.5 ± 9.1%	8.3 ± 7.7%
Limestone	3.9 ± 3.7%	4.6 ± 4.5%	4.4 ± 4.0%	4.8 ± 4.3%
Dolomite	8.0 ± 7.4%	10.0 ± 9.5%	7.6 ± 7.1%	6.5 ± 9.0%

GM: geometric mean; AM: arithmetic mean; H&S: Hashin and Shtrikman.

Table 3 compares the errors after applying correction charts to the various mean models with the errors resulting from utilizing the new conversion equations. Considering all samples, the implementation of correction charts resulted in the smallest error for the arithmetic mean. If lithotypes are concerned, the fit of all these approaches is good for every mixing model, except for the geometric mean applied to sandstone. This misfit is a consequence of the high porosity of the sandstone samples (19.8 ± 8.8%), combined with the mathematical structure of the geometric mean.

For all lithotypes, both the correction equations for the mean models and the conversion equations yield to uncertainties in the BTC ranging between 5% and 10% (AME). These uncertainties are significantly better than those arising from application of the mean models without correction (range of AME 11–42%).
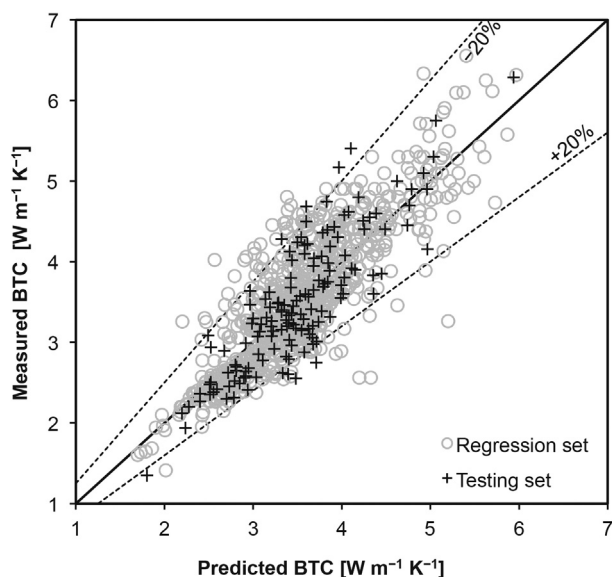
7. Conclusions

In both the general geothermal characterization of sedimentary basins, including the assessment of geothermal reservoirs, as well as the modeling of other potential resources, for example oil and gas, the implementation of large numbers of BTC data is required. In the light of the time-extensive effort necessary to determine water-saturated TC for such large sample sets, methods are requested to reduce the work load. The mean models for BTC of two-phase rocks presented and evaluated in this study constitute efficient tools to transfer air-saturated BTC to water-saturated BTC, if porosity is known from independent sources (e.g., derived from standard well logs). If a correction equation (see Section 6.2) is applied to the mean model result, the errors in water-saturated BTC can be reduced to 4–11%, depending on lithotype. In turn, the application of model-independent conversion equations (reported in Section 6.3) allows a general reduction of the error to <10%. This accuracy is sufficient for many industrial as well as specific scientific applications.

The more sophisticated physical rock models, that are advanced effective-medium theory models, require knowledge of additional rock parameters that are not readily available. Acquisition of such additional parameters (for instance, distribution and size of grains and pores) is labor-intensive and requires special analytical equipments. Therefore, such models are suitable for basic research, but are unlikely to be routinely used in exploration studies.

It remains to be investigated whether the TC measuring technique, on which the data evaluated in this study are based and which do not apply pressure to the sample, eventually underestimates the measured TC, and whether these effects are statistically relevant to alter the equations and correction charts developed in this study. In addition, laboratory studies are required to eliminate the ambiguity in pressure dependency of TC in the range <10 MPa. This would also shed light on the reasoning of the small deviation between DB and OS values recognized by Popov et al. (1999), implying a pressure dependency of TC that is much smaller than reported by other authors (e.g., Buntebarth, 1991; Hurtig and Brugger, 1970; Kukkonen et al., 1999; Somerton et al., 1963; Walsh and Decker, 1966). Unless those ambiguities are overcome, we consider our results as universal for application for isotropic to weakly anisotropic sedimentary rocks.

Fig. 9. Scatter plot of predicted (conversion equation based on multiple regression analysis) vs. measured water-saturated BTC.

References

Abdulagatova, Z.Z., Abdulagatov, I.M., Emirov, S.N., 2009. Effect of temperature and pressure on the thermal conductivity of sandstone. International Journal of Rock Mechanics and Mining Sciences 46, 1055–1071.

Balling, N., Kristiansen, J., Breiner, N., Poulsen, K.D., Rasmusen, R., Saxov, S., 1981. Geothermal Measurements and Subsurface Temperature Modelling in Denmark, vol. 16. Geologiske Skrifter, Department of Geology Aarhus University, 172 pp.

Beck, A.E., 1988. Methods for determining thermal conductivity and thermal diffusivity. In: Haenel, et al. (Eds.), Handbook of Terrestrial Heat-Flow Density Determination. Kluwer Academic Publishers, Dordrecht, Netherlands, pp. 87–124.

Beck, J.M., Beck, A.E., 1965. Computing thermal conductivities of rocks from chips and conventional specimens. Journal of Geophysical Research 70, 5227–5239.

Birch, F., 1950. Flow of heat in the Front Range, Colorado. Bulletin of the Geological Society America 61, 567–630.

Blackwell, D.D., Steele, J.L., 1989. Thermal conductivity of sedimentary rocks: measurement and significance. In: Naeser, N.D., McCulloh, T.H. (Eds.), Thermal History of Sedimentary Basins, Methods and Case Histories. Springer, New York, pp. 13–35.

Brailsford, A.D., Major, K.G., 1964. The thermal conductivity of aggregates of several phases, including porous material. British Journal of Applied Physics 15, 313–319.

Brigaud, F., Chapman, D.S., Le Douran, S., 1990. Estimating thermal conductivity in sedimentary basins using lithological data and geophysical well logs. AAPG Bulletin 74, 1459–1477.

Bruggeman, D.A.G., 1935. Berechnung verschiedener Konstanten von heterogenen Substanzen – I. Dielektrizitätskonstanten und Leitfähigkeiten der Mischkörper aus isotropen Substanzen. Annalen der Physik 24, 636–679.

Budavari, S., 1989. The Merck Index – Encyclopedia of Chemicals, Drugs and Biologicals. Merck and Co., Inc., Rahway, New Jersey, 817 pp.

Buntebarth, G., 1991. Thermal properties of KTB Oberpfalz VB core samples at elevated temperature and pressure. Scientific Drilling 2, 73–80.

Buntebarth, G., Schopper, J.R., 1998. Experimental and theoretical investigations on the influence of fluids, solids and interactions between them on thermal properties of porous rocks. Physics and Chemistry of the Earth 23, 1141–1146.

Carson, J.K., Lovatt, S.J., Tanner, D.J., Cleland, A.C., 2005. Thermal conductivity bounds for isotropic, porous materials. International Journal of Heat and Mass Transfer 48, 2150–2158.

Clauser, C., 2006. Geothermal energy. In: Heinloth, K. (Ed.), Advanced Materials and Technologies. Landolt-Börnstein, Group VIII, Energy Technologies, Subvol. C: Renewable Energies, Vol. 3. Springer Verlag, Heidelberg/Berlin, p. 541.

Clauser, C., 2009. Heat transport processes in the earth's crust. Surveys in Geophysics 30, 163–191.

Clauser, C., Hartmann, A., Koch, A., Mottaghy, D., Pechnig, R., Rath V., 2007. Erstellung statistisch abgesicherter thermischer und hydraulischer Gesteinseigenschaften für den flachen und tiefen Untergrund in Deutschland, Phase 1 – Westliche Molasse und nördlich angrenzendes Süddeutsches Schichtstufenland. Final report for BMU-Project FKZ 0329985, RWTH Aachen, http://www.eonerc. rwth-aachen.de/aw/cms/website/zielgruppen/gge/research_gge/geothermik/ ~vfa/Erstellung_statistisch_abgesicherter_thermischer/ (last accessed: 21.03.13).

Demongodin, L., Pinoteau, B., Vasseur, G., Gable, R., 1991. Thermal conductivity and well logs: a case study in the Paris Basin. Geophysical Journal International 105, 675–691.

Eucken, A., 1940. Allgemeine Gesetzmäßigkeiten für das Wärmeleitvermögen verschiedener Stoffarten und Aggregatzustände. Forschung auf dem Gebiete des Ingenieurwesens, Ausgabe A 11 (1), 6–20.

Fuchs, S., Förster, A., 2010. Rock thermal conductivity of Mesozoic geothermal aquifers in the Northeast German Basin. Chemie der Erde 70 (Suppl. 3), 13–22.

Goss, R.D., Combs, J., 1976. Thermal Conductivity Measurement and Prediction from Geophysical Well Log Parameters with Borehole Application. Institute for Geosciences, University of Texas at Dallas, Dallas, pp. 1019–1027.

Goutorbe, B., Lucazeau, F., Bonneville, A., 2006. Using neural networks to predict thermal conductivity from geophysical well logs. Geophysical Journal International 166, 115–125.

Gröber, H., Erk, S., Grigull, U., 1955. Die Grundgesetze der Wärmeübertragung, 2nd ed. Springer, Berlin, Wien, Heidelberg, 465 pp.

Hanai, T., 1968. Electrical properties of emulstons. In: Sherman, P. (Ed.), Emulsion Science. Academic Press, New York, pp. 354–477.

Hartmann, A., Rath, V., Clauser, C., 2005. Thermal conductivity from core and well log data. International Journal of Rock Mechanics and Mining Sciences 42, 1042–1055.

Hartmann, A., Pechnig, R., Clauser, C., 2008. Petrophysical analysis of regional-scale thermal properties for improved simulations of geothermal installations and basin-scale heat and fluid flow. International Journal of Earth Sciences 97, 421–433.

Hashin, Z., Shtrikman, S., 1962. A variational approach to the theory of the effective magnetic permeability of multiphase materials. Journal of Applied Physics 33, 3125–3131.

He, L., Hu, S., Huang, S., Yang, W., Wang, J., Yuan, Y., Yang, S., 2008. Heat flow study at the Chinese Continental Scientific Drilling site: borehole temperature, thermal conductivity, and radiogenic heat production. Journal of Geophysical Research 113 (B02404), http://dx.doi.org/10.1029/2007JB004958.

Homuth, S., Sass, I., Hamm, K., Rumohr, S., 2008. In-Situ-Messungen zur Bestimmung geothermischer Untergrundkennwerte. Grundwasser 13, 241–251.

Horai, K.-I., 1991. Thermal conductivity of Hawaiian basalt: a new interpretation of Robertson and Peck's data. Journal of Geophysical Research 96, 4125–4132.

Hurtig, E., Brugger, H., 1970. Wärmeleitfähigkeitsmessung unter einaxialem Druck. Tectonophysics 10, 67–77.

Hutt, J.R., Berg, J.W., 1968. Thermal and electrical conductivities of sandstone rocks and ocean sediments. Geophysics 33, 489–500.

Kappelmeyer, O., Haenel, R., 1974. Geothermics with Special Reference to Application. Geopublication Associates, Geoexploration Monographs, Gebrüder Borntraeger Berlin, Series 1, No. 4., 238 pp.

Kukkonen, I.T., Jokinen, J., Seipold, U., 1999. Temperature and pressure dependencies of thermal transport properties of rocks: implications for uncertainties in thermal lithosphere models and new laboratory measurements of high-grade rocks in the Central Fennoscandian Shield. Surveys in Geophysics 20, 33–59.

Lemmon, E.W., McLinden, M.O., Friend, D.G., 2005. Thermophysical properties of fluid systems. In: Linstrom, P.J., Mallard, W.G. (Eds.), NIST Chemistry WebBook, NIST Standard Reference Database, Number 69. National Institute of Standards and Technology, Gaithersburg, MD, p. 20899, http://webbook.nist.gov (last accessed: 21.02.13).

Lewis, T., Villinger, H., Davis, E., 1993. Thermal conductivity measurement of rock fragments using a pulsed needle probe. Canadian Journal of Earth Sciences 30, 480–485.

Lichtenecker, K., 1924. Der elektrische Leitungswiderstand künstlicher und natürlicher Aggregate, vol. 25. Physikalische Zeitschrift, pp. 169–181, 193–204, 226–233.

Liu, S., Feng, C., Wang, L., Cheng, L., 2011. Measurement and analysis of thermal conductivity of rocks in the Tarim Basin, Northwest China. Acta Geologica Sinica – English Edition 85, 598–609.

Majorowicz, J., Šafanda, J., Torun-1 Working Group, 2008. Heat flow variation with depth in Poland: evidence from equilibrium temperature logs in 2.9-km-deep well Torun-1. International Journal of Earth Sciences 97, 307–315.

Maxwell, J.C., 1892. A Treatise on Electricity and Magnetism, vol. 440., 3rd ed. Clarendon Press 1, Oxford, UK, 425 pp.

Mottaghy, D., Schellschmidt, R., Popov, Y.A., Clauser, C., Kukkonen, I.T., Nover, G., Milanovsky, S., Romushkevich, R.A., 2005. New heat flow data from the immediate vicinity of the Kola super-deep borehole: vertical variation in heat flow confirmed and attributed to advection. Tectonophysics 401, 119–142.

Norden, B., Förster, A., 2006. Thermal conductivity and radiogenic heat production of sedimentary and magmatic rocks in the Northeast German Basin. AAPG Bulletin 90, 939–962.

Orilski, J., Schellschmidt, R., Wonik, T., 2010. Temperaturverlauf und Wärmeleitfähigkeit im Untergrund der Bohrung Groß Buchholz GT1 in Hannover. Extended Abstract, Geothermiekongress 2010. 17.–19.11.2010, Karlsruhe, p. 10.

Popov, Y.A., Tertychnyi, V., Romushkevich, R., Korobkov, D., Pohl, J., 2003. Interrelations between thermal conductivity and other physical properties of rocks: experimental data. Pure and Applied Geophysics 160, 1137–1161.

Popov, Y.A., Pevzner, L.A., Rumushkevich, R.A., Korostelev, V.M., Vorob'jev, M.G., 1995. Thermophysical and geothermal sections obtained from Kolvinskaya well logging data. Physics of the Solid Earth, English Translation 30, 778–789.

Popov, Y.A., Pribnow, D.F.C., Sass, J.H., Williams, C.F., Burkhardt, H., 1999. Characterization of rock thermal conductivity by high-resolution optical scanning. Geothermics 28, 253–276.

Popov, Y.A., Miklashevskiy, D., Romushkevich, R., Novikov, S., Parshin, A., Safonov, S., 2010. Proceedings of the World Geothermal Congress , Bali, Indonesia, 25–29 April, p. 9.

Popov, Y.A., Romushkevich, R., Korobkov, D., Mayr, S., Bayuk, I., Burkhardt, H., Wilhelm, H., 2011. Thermal properties of rocks of the borehole Yaxcopoil-1 (Impact Crater Chicxulub, Mexico). Geophysical Journal International 184, 729–745.

Pribnow, D.F.C., 1994. Ein Vergleich von Bestimmungsmethoden der Wärmeleitfähigkeit unter Berücksichtigung von Gesteinsgefügen und Anisotropie. VDI Fortschrittsberichte Reihe 19(75), VDI-Verlag, Düsseldorf, Germany, 111 pp.

Progelhof, R.C., Throne, J.L., Ruetsch, R.R., 1976. Methods for predicting the thermal conductivity of composite systems: a review. Polymer Engineering & Science 16, 615–625.

Reuss, A., 1929. Berechnung der Fließgrenze von Mischkristallen auf Grund von Plastizitätsbedingung für Einkristale. Zeitschrift für Angewandte Mathematik und Mechanik 9, 49–58.

Revil, A., 2000. Thermal conductivity of unconsolidated sediments with geophysical applications. Journal of Geophysical Research 105, 16749–16768.

Robertson, E.C., Peck, D.L., 1974. Thermal conductivity of vesicular basalt from Hawaii. Journal of Geophysical Research 79, 4875–4888.

Schärli, U., Rybach, L., 1984. On the thermal conductivity of low-porosity crystalline rocks. Tectonophysics 103, 307–313.

Schön, J.-H., 1996. Physical properties of rocks, fundamentals and principles of petrophysics. In: Treitel, S., Helbig, K. (Eds.), Handbook of Geophysical Exploration: Seismic Exploration, vol. 18. Pergamon, Oxford, UK, p. 583.

Schopper, J.R., 1991. An amendment to Gassmann's theory. In: Proceedings of the 14th SPWLA European Formation Evaluation Symposium, December 9–11, London, England, 19 pp.

Schütz, F., Norden, B., Förster, A., DESIRE Group, 2012. Thermal properties of sediments in southern Israel: a comprehensive data set for heat flow and geothermal energy studies. Basin Research 24, 357–376.

Sen, P.N., Scala, C., Cohen, M.H., 1981. A self-similar model for sedimentary rocks with application to the dielectric constant of fused glass beads. Geophysics 46, 781–795.

Somerton, W.H., 1992. Thermal Properties and Temperature-Related Behavior of Rock/Fluid Systems. Elsevier Science Publishers B.V., Amsterdam, 257 pp.

Somerton, W.H., Ward, S.H., King, M.S., 1963. Physical properties of Mohole test site basalt. Journal of Geophysical Research 68, 849–856.

Sugawara, A., Yoshizawa, Y., 1961. An investigation on the thermal conductivity of porous materials and its application to porous rock. Australian Journal of Physics 14, 469–480.

Tinga, W.R., Voss, W.A.G., Blossey, D.F., 1973. Generalized approach to multiphase dielectric mixture theory. Journal of Applied Physics 44, 3897–3902.

Vasseur, G., Brigaud, F., Demongodin, L., 1995. Thermal conductivity estimation in sedimentary basins. Tectonophysics 244, 167–174.

Voigt, W., 1928. Lehrbuch der Kristallphysik. Teubner, Leipzig, 978 pp.

Walsh, J.B., Decker, E.R., 1966. Effect of pressure and saturating fluid on the thermal conductivity of compact rock. Journal of Geophysical Research 71, 3053–3061.

Watanabe, H., 2003. Thermal conductivity and thermal diffusivity of sixteen isomers of alkanes: C_nH_{2n+2} ($n = 6$ to 8). Journal of Chemical and Engineering Data 48, 124–136.

Wiener, O.H., 1912. Die Theorie des Mischkörpers für das Feld der stationären Strömung, Erste Abhandlung: Die Mittelwertsätze für Kraft, Polarisation und Energie. Abhandlungen der mathematisch-physischen Klasse der Königlich-Sächsischen Gesellschaft der Wissenschaften 32, 507–604.

Woodside, W., Messmer, J., 1961a. Thermal conductivity of porous media. I. Unconsolidated sands. Journal of Applied Physics 32, 1688–1699.

Woodside, W., Messmer, J., 1961b. Thermal conductivity of porous media. II. Consolidated rocks. Journal of Applied Physics 32, 1699–1706.

Zimmerman, R.W., 1989. Thermal conductivity of fluid-saturated rocks. Journal of Petroleum Science and Engineering 3, 219–227.